Dichroic Plasmonic Films based on Anisotropic Au Nanoparticles for Enhanced Sensitivity and Figure of Merit Sensing

SUPPORTING INFORMATION

*William L. Watkins, Antonio Assaf, Geoffroy Prévot, Yves Borensztein**

Sorbonne Université, CNRS, Institut des NanoSciences de Paris, INSP, F-75005, Paris, France

* Corresponding Author : yves.borensztein@insp.jussieu.fr

Part SI.1 Additional SEM and optical data

a. Large scale SEM images of samples I, II and III.

Figures S.1 gives micrometer scale SEM images of samples (I), (II) and (III), investigated in the main article. The gold films were elaborated at 310 K and with a grazing incidence equal to 12°. The average deposition rate was 0.024 ± 0.004 nm/s. In spite of some local inhomogeneities, likely due to some imperfections of the glass surface cleaning, the gold NP films display a satisfying homogeneity at the micrometer scale.

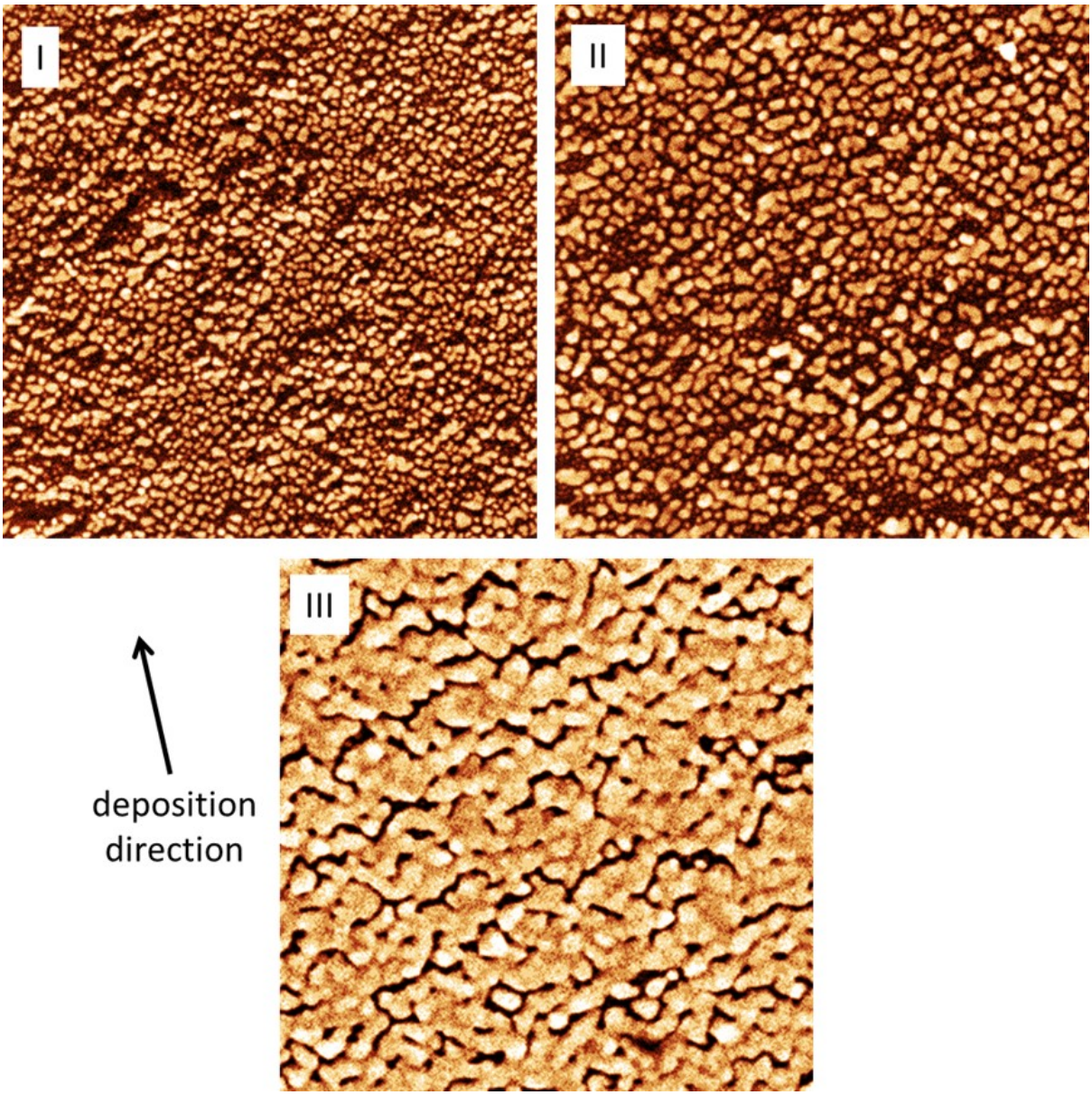

Fig. S.1. SEM images of samples (I), (II) and (III). Size: 1000 nm x 1000 nm.

b. Additional samples

SEM images

Fig.S.2. shows SEM images of three other samples (V) to (VII) prepared in close conditions to samples (I) to (III) of the main article and of Fig.S.1. The grazing angle was a little larger (16° vs. 12°), the temperature during the deposit was 310 K, and the mass thicknesses were 6.5, 12.2 and 18.6 nm, respectively. The average deposition rate was 0.031 ± 0.005 nm/s. The general morphologies are similar to those of samples (I) to (III) of the main article, showing actually a more homogeneous structure than those presented in Fig.S.1, likely due to glass slides with no or less imperfections. Sample (V) is an island-film type sample, intermediate between samples (I) and (II). Sample (VII), almost continuous, is a percolated strip type sample, similar to sample (III). Sample (VI) is intermediate between the island film and the percolated film.

Optical response

The transmission spectra measured parallel and perpendicular to the deposition directions, for samples V and VII, are quite similar to the spectra obtained on samples I and III. In the former case (V), two well-defined LSPR are observed, corresponding to the resonance with the NPs, in their short and long dimension. In the latter case, no resonance is visible in the normal direction, as was observed for samples III, and a weak and broad resonance in the parallel direction, which is the LSPR in the grooves separating the percolated islands. This is quite identical to what is shown for samples (I) and (II) on the one hand, and (III) on the other hand (Figure 5 of the main article). The optical response of sample VI is also intermediate between those of samples V and VII.

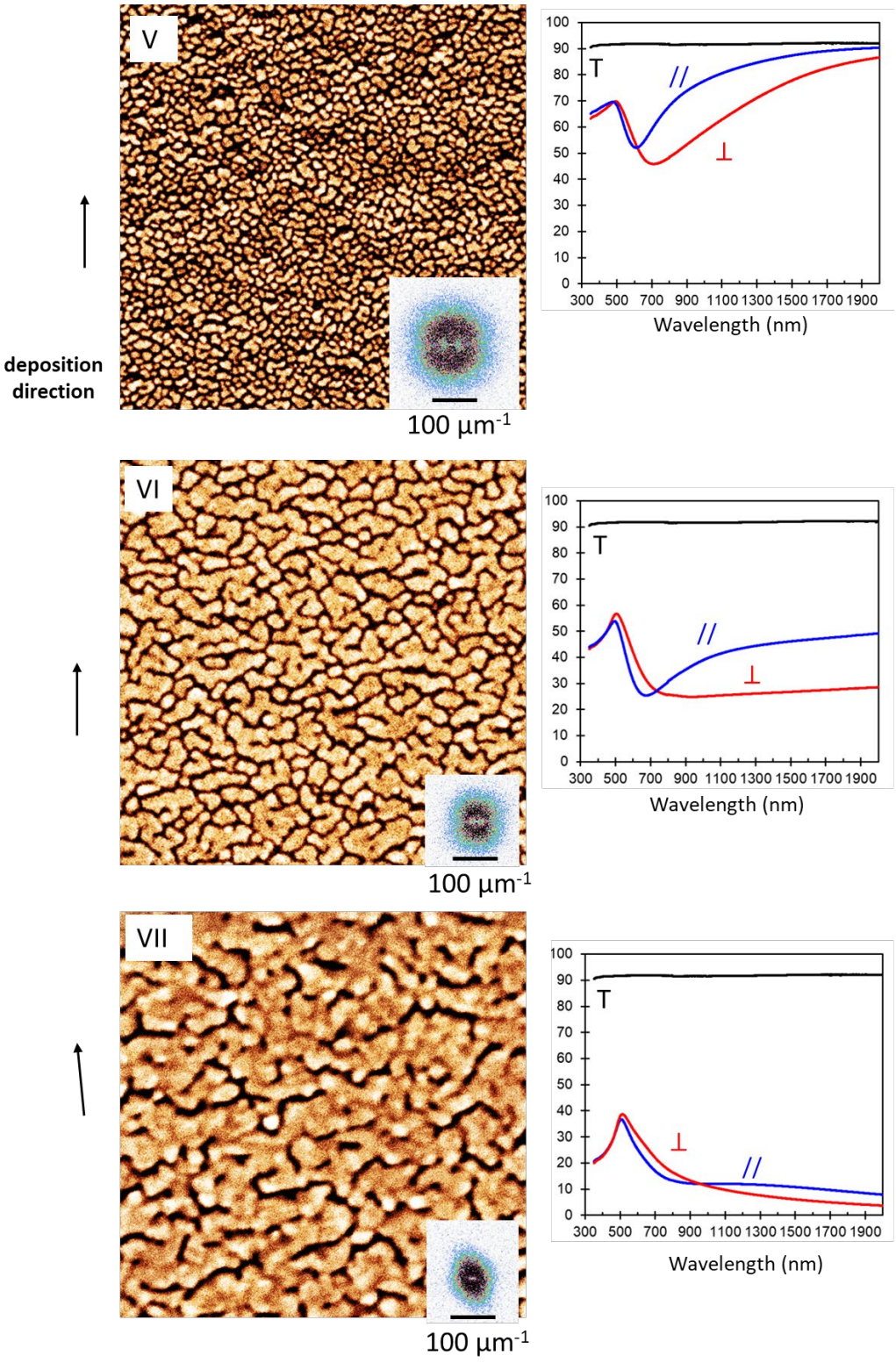

Fig. S.2. Samples (V) to (VII). SEM images (1000 nm x 1000 nm) and corresponding Fourier transforms. Transmittance spectra of glass (black) and of the gold films, with polarization parallel (blue) and perpendicular (red) to the deposition direction. Temperature of the glass slides during deposition: 310 K. Angle of deposition: 16°; mass thicknesses of samples (V), (VI) and (VII): 6.5, 12.2 and 18.6 nm, respectively.

c. Effect of the grazing deposition angle.

Figure S.3 show the SEM images and the corresponding transmission spectra obtained on two samples with close mass thicknesses: 8.5 nm and 7.5 nm for samples (a) and (b), elaborated at 310 K with 32° and 12° grazing incidence, respectively. The deposition rates were 0.049 and 0.032 nm/s, respectively. Sample (a) shows no clear morphological anisotropy, contrarily to sample (b) which displays a slight anisotropy, as evidenced by the Fourier transform diagram of the SEM images. The transmission and the TA spectra show the optical anisotropy of both samples, which is larger for sample (b) than for sample (a), even although the amount of gold of (b) is slightly smaller. The transmission spectra have been recorded with a spectrophotometer different than the one used for samples I to IV in the main article, and for samples V to VII covering only the 300-1100 nm range.

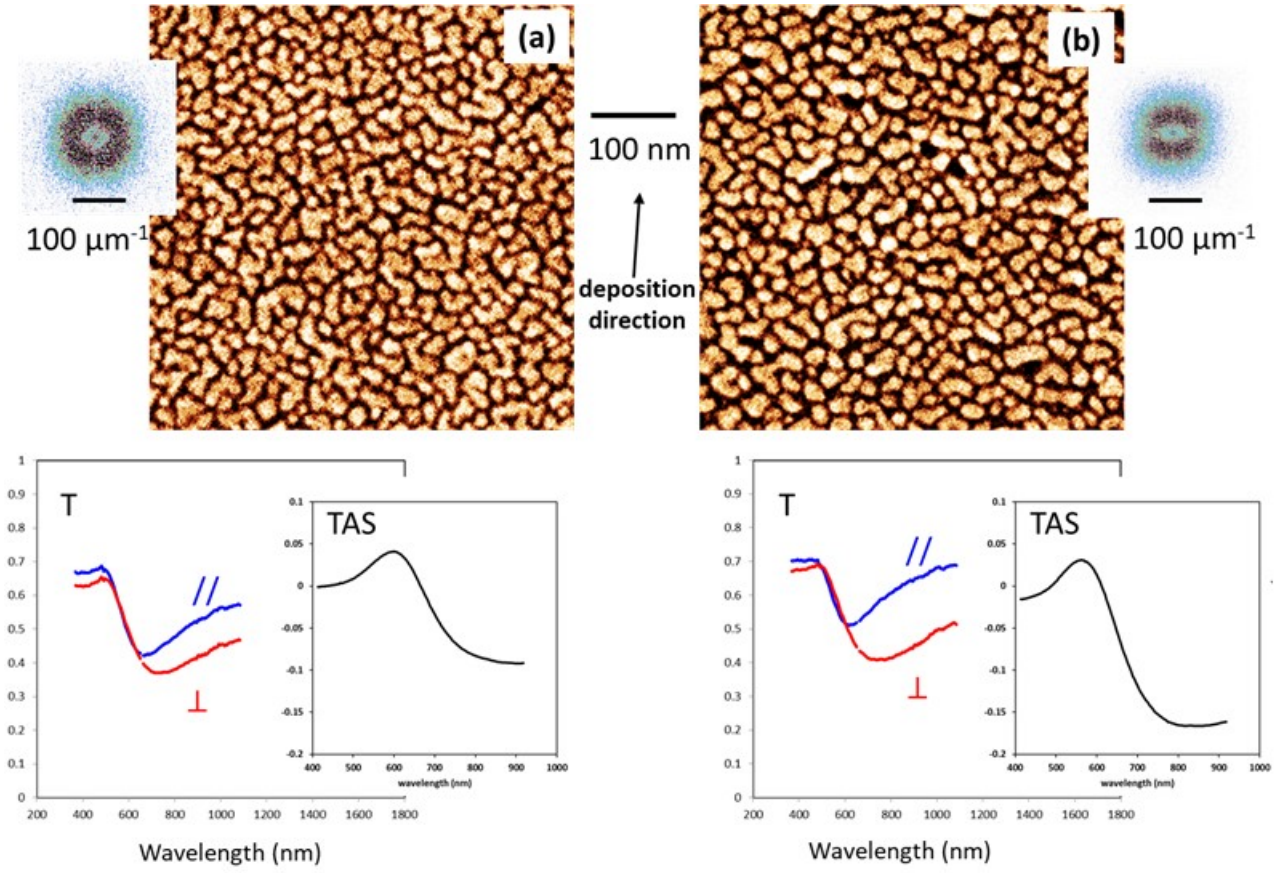

Figure S.3. SEM images (500 nm x 500 nm) measured on two samples (a) and (b), deposited at 310 K, with mass thicknesses equal to 8.5 nm and 7.5 nm and grazing angles of 32° and 12°, respectively. Corresponding transmission spectra parallel and normal to the deposition direction, and corresponding Transmission Anisotropy Spectra.

d. Effect of post-annealing

The samples used in this article are typically post-annealed at temperature ranging from 120°C to 140 °C for 10 minutes, in order to favor a better stability with time. This annealing does not modify the shape and the distribution of the NPs, nor their optical anisotropy. Fig S.4(a) and (b) show two SEM images on the same sample before and after annealing at 140°C, which do not display any obvious morphological change.

On the contrary, annealing at a temperature higher than ca. 140°C induces a coarsening of the NP assembly and a rounding of their shape, as it has been shown in detail by previous investigations for samples elaborated at normal incidence [1]. As observed in those articles, this induces a blue shift of the LSPR, and in our case, a decrease of their optical anisotropy. Figure S.4(c) indeed shows the TAS measured on the same sample. Annealing at 110°C increases a little the anisotropy, which may be due some coalescence of particles along the direction perpendicular to the deposition direction. A very slight blue shift starts at 140 °C, which becomes larger for temperatures of 180°C and 220 °C, together with a strong decrease of the anisotropy, making the samples less adapted to the present anisotropy measurements. This is related to the progressive change of the shape of the NPs towards their equilibrium shape.

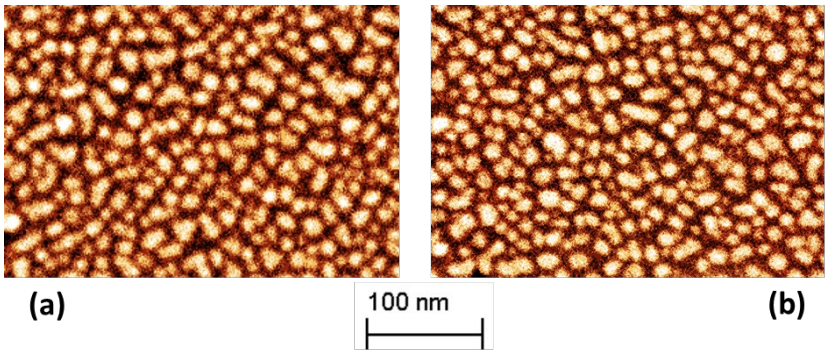

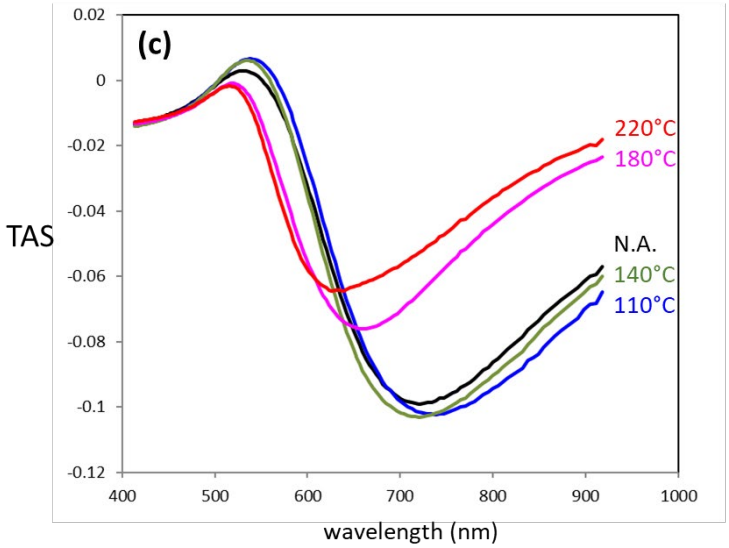

Fig.S.4. (a) and (b) SEM image of a sample, prepared by deposition with a grazing angle of 12°, at substrate temperature of 310 K and rate of deposition equal to 0.05 nm/s, before and after annealing at 140°C during 10 min. The mass thickness is equal to 4.1 nm. (c) TAS spectra measured on the non-annealed sample (N.A.) and after increasing annealing temperatures.

Part SI.2. Transmission Anisotropy Spectrometer set-up

The TAS apparatus is based on the Reflectance Anisotropy Spectrometer developed by Aspnes and col., and we use the same set-up as the one described in details in the reference [2]. It is schematized in Figure S.5. After being polarized normally to the working plane (here, the sheet plane), the beam passes twice through the sample and the cell, being reflected by a mirror at the rear. The sample is oriented at 45° with respect to the polarization of light. The reflected light is analyzed by means of a Photo-Elastic Modulator, working at 50 kHz coupled with another polarizer, playing the role of an analyzer. It is then dispersed by a monochromator, and the signal measured by the photomultiplier located at the exit slit of the monochromator is analyzed by use of a lock-in amplifier.

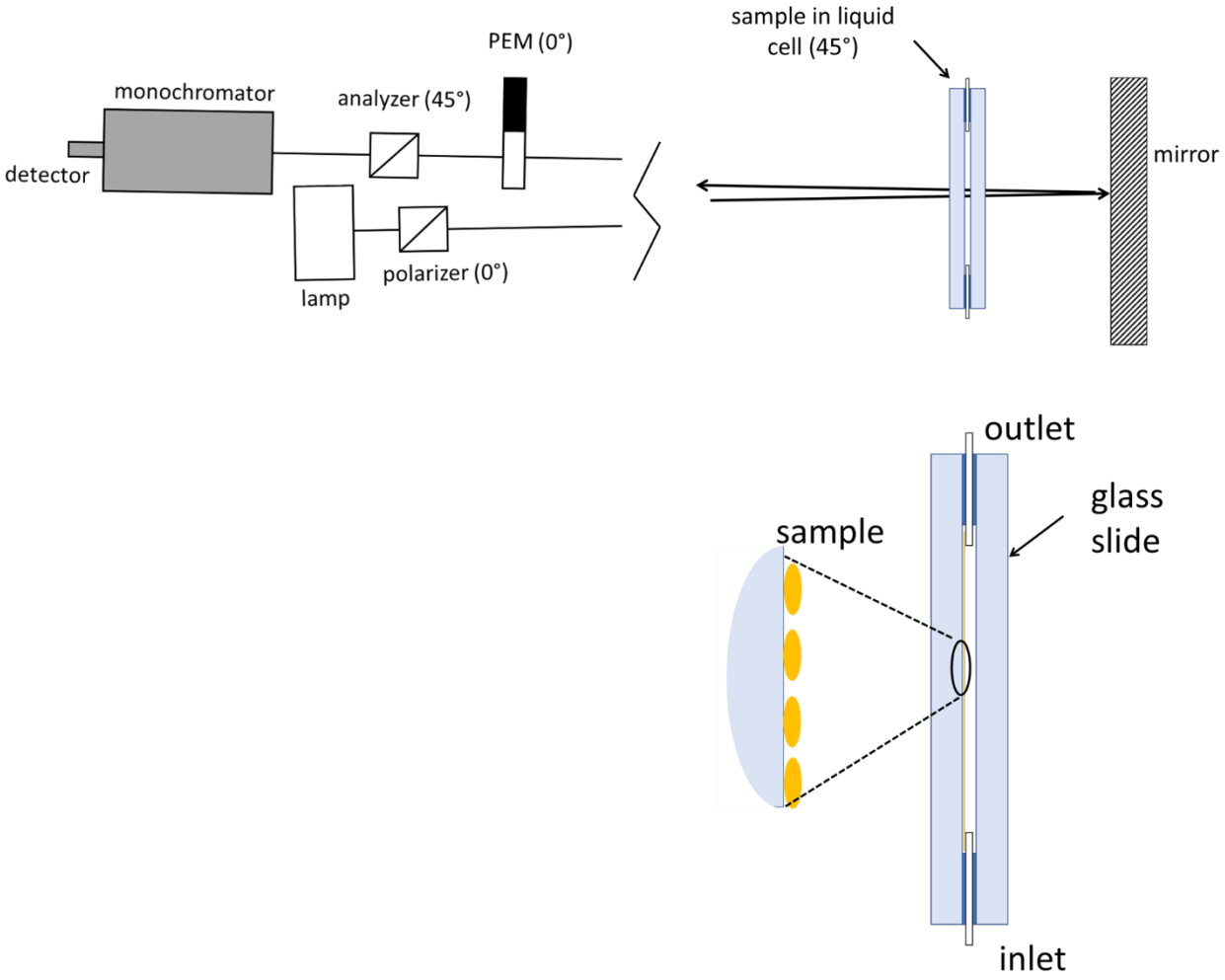

Fig.S.5. Scheme of the TAS set-up and of the liquid cell.

Part SI.3. Evolution of the film morphology: Monte Carlo results

In this part, we show the effect, on the morphology of a 5 nm thick film corresponding to sample (I) of the main article, of the free parameters in play in the Monte Carlo calculation: $E_{diff-glass}$, $E_{diff-gold}$, E_{E-S}, $E_{b-glass}$, E_{b-gold} and $E_{Au-glass}$. All the corresponding simulations have been performed for a 256×256 square lattice corresponding to $65.7 \times 65.7\ nm^2$.

The set of parameters corresponding to these simulations is given in table S1. In addition to the input parameters, we also give the difference of the binding energies, ΔE_b, for an atom located on the substrate at the edge of a gold NP, and for an isolated atom on top of the NP. The results of the calculations are given in Fig.S.6

A general observation is that the shape of the NPs is mainly related to this energy difference ΔE_b. The larger the difference, the more difficult it is for the Au atoms to jump up the NPs and the flatter the NPs are. The best fitting of our experimental results corresponds to an energy difference of 0.188 eV (case 7). The different changes of the parameters, taken equal to about 10 to 20%, lead to changes in this difference and therefore to shapes and distributions of the NPs different from the experimental observation.

Table S.1

Case	T	ν_o	$E_{diff-glass}$ (eV)	$E_{diff-gold}$ (eV)	E_{E-S} (eV)	$E_{b-glass}$ (eV)	E_{b-gold} (eV)	$E_{Au-glass}$ (eV)	ΔE_b (eV)
1	310 K	10^{12} s^{-1}	0.23	0.14	0.03	0.7	0.65	0.078	0.128
2	310 K	10^{12} s^{-1}	0.23	0.14	0.03	0.65	0.59	0.078	0.138
3	310 K	10^{12} s^{-1}	0.18	0.14	0.03	0.7	0.59	0.043	0.153
4	310 K	10^{12} s^{-1}	0.23	0.17	0.03	0.7	0.59	0.057	0.167
5	310 K	10^{12} s^{-1}	0.23	0.14	0.03	0.7	0.59	0.063	0.173
6	310 K	10^{12} s^{-1}	0.23	0.14	0.06	0.7	0.59	0.078	0.188
7 (best fitting)	**310 K**	**10^{12} s^{-1}**	**0.23**	**0.14**	**0.03**	**0.7**	**0.59**	**0.078**	**0.188**
8	310 K	10^{12} s^{-1}	0.23	0.14	0.00	0.7	0.59	0.078	0.188
9	310 K	10^{12} s^{-1}	0.23	0.14	0.03	0.7	0.59	0.093	0.203
10	310 K	10^{12} s^{-1}	0.23	0.11	0.03	0.7	0.59	0.099	0.209
11	310 K	10^{12} s^{-1}	0.28	0.14	0.03	0.7	0.59	0.113	0.223
12	310 K	10^{12} s^{-1}	0.23	0.14	0.03	0.7	0.53	0.078	0.248

13	310 K	10^{12} s^{-1}	0.23	0.14	0.03	0.77	0.59	0.078	0.258

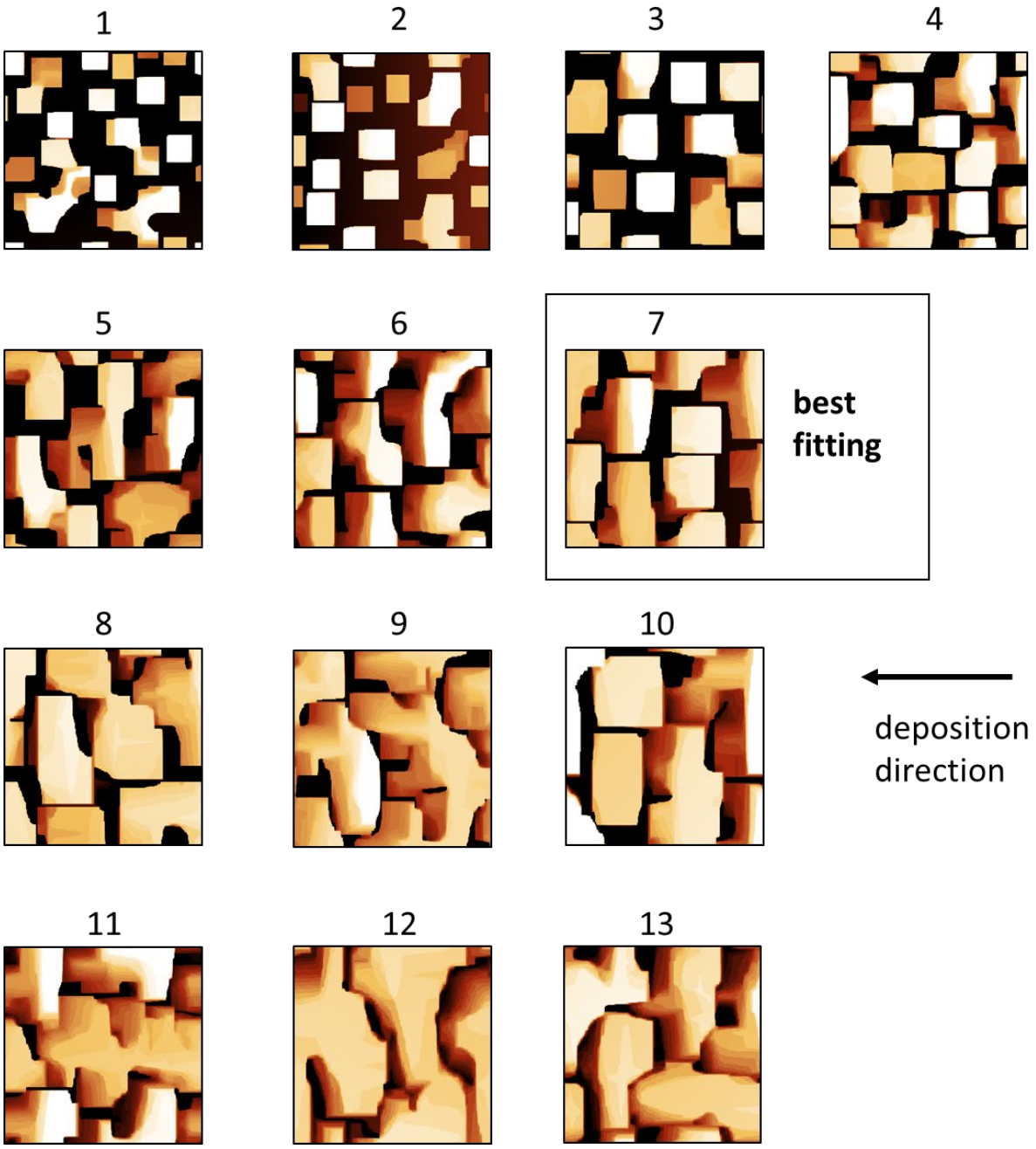

Fig.S.6. Morphology calculated for different Monte Carlo parameters given in Table S.1, indicated by the case number. Size $65.7 \times 65.7\ nm^2$

Part SI.4. Modification of the dielectric function of gold for taking account the small size of the NPs.

The effective mean free path of the conduction electrons, equal to 12.8 nm in bulk, is reduced in a nanoparticle, because of electron scattering at its surface. The experimental dielectric function for gold $\varepsilon_{Au}^{bulk}(\omega)$, taken from Ref [3], is therefore modified in the following way [4] :

$$\varepsilon_{Au}^{\mathrm{mod}}(\omega) = \varepsilon_{Au}^{bulk}(\omega) + \frac{\Omega_p^{\,2}}{\omega\left(\omega + i\,\tau_{bulk}^{-1}\right)} - \frac{\Omega_p^{\,2}}{\omega\left(\omega + i\,\tau_{\mathrm{mod}}^{-1}\right)} \qquad \text{(Eq.S1)}$$

where

$$\Omega_p = \left(\frac{Ne^2}{\varepsilon_o m}\right)^{\frac{1}{2}} \qquad \text{(Eq.S2)}$$

is the Drude plasma frequency of the conduction s-p electrons in gold, that is the value of the plasma frequency which does not account for the screening due to the "bound" electrons, i.e. the effect of the interband transitions. Here N is the density of conduction electrons, e their charge and m their effective mass, all in SI units. For gold, $\hbar\Omega_p$ = 9.04 eV. τ_{mod} denotes the relaxation time of the conduction electrons in the Au NPs. It differs from its value τ_{bulk} in gold bulk, because of the reduced mean free path given by $l_{mod} = v_{Fermi}\,\tau_{mod}$. For Au nanospheres, the modified free mean path can be written [5]:

$$l_{mod}^{-1} = l_{bulk}^{-1} + \frac{A}{R} \qquad \text{(Eq.S3)}$$

where R is the radius of the spheres and A is a phenomenological parameter, whose value ranges between about 0.1 and 1.5, depending on the theories describing the LSPR in the particle. In the present case, for ellipsoidal NPs of sizes given in Table 2 of the main article, we have taken A=1 and an equivalent radius R=13 nm, for all the calculations, except for Fig.7, where the equivalent radius was taken equal to the length b for every NP.

Part SI.5. Sensitivity and stability of the TAS apparatus. Discussion of the FoM*

Fig.S.7 shows the evolution of the signal $I = TA$, initially fixed at the value 0, as a function of time and after several rotations of the polarizer, measured at 700 nm on a gold anisotropic sample. The noise of the recorded signal is about $0.5\ 10^{-5}$. It depends of course on the integration time, which was chosen here equal to 10 sec. There is also a continuous signal drift of about $1.4\ 10^{-5}$ per hour.

The rotating polarizer holder was a high-precision mechanical rotation stage from MKS Newport, simply modified to increase its sensitivity around 0.1 arcsec. The changes of the polarizer angle during registration of the signal in Fig.S7 were equal to 0.3 arcsec at times 20, 60, 80 min and to 0.6 arcsec at time 150 min, leading to changes equal to about -1.10^{-5} and -2.10^{-5} respectively; the uncertainty ε on the signal I due to the precision of the polarizer angle is therefore about $0.5\ 10^{-5}$.

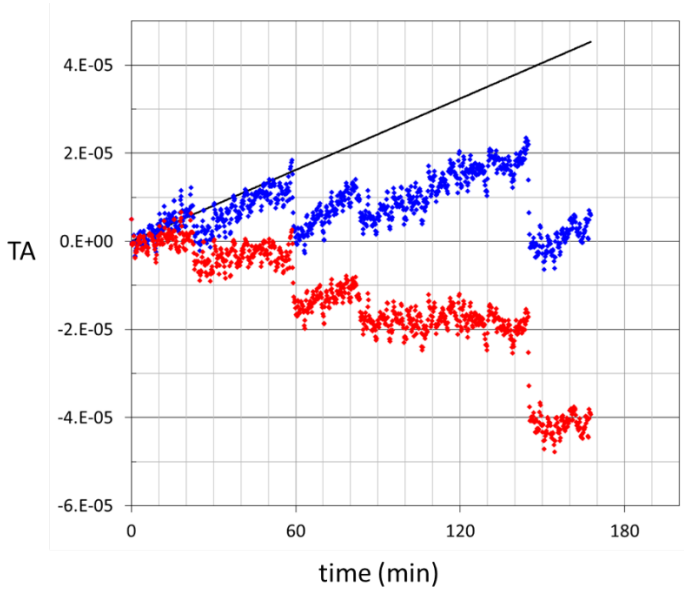

Fig. S.7. Blue dots: signal I=TA recorded during time. Continuous black line: drift which is suppressed from the signal during analysis, in order to obtain the drift-less signal drawn in red.

This shows that, with the present conditions, the signal can be fixed at zero and stays fixed at this value for one hour, with a total accuracy better than to 2.10^{-5}. With these values, it would lead to a FoM* equal to $0.7/2.10^{-5} = 35\,000\ \mathrm{RIU}^{-1}$. In the main paper, based on the results of Fig.6, the theoretical FoM* was calculated equal to 23 000.

Part SI.6. Determination of the FWMH of the TA spectrum

Figure S.8 shows the TA spectrum measured on sample (IV) in water together with its absolute value. The FWMH of the latter spectrum can be determined, and its value is measured here equal to 90 nm**.**

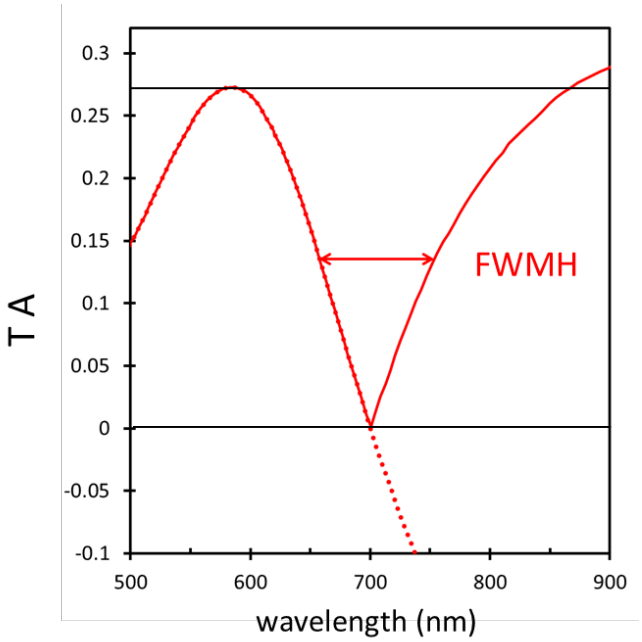

Fig. S.8. Dotted line: TA spectrum of sample (IV) measured in water ; continuous line: Absolute value of TA.

Part SI.7. "Demonstration" of Eq.8

We show here that Eq.8 of the main article:

$$\Delta\lambda = S\,(n_s - n_{med})\left[1 - \left(\frac{l_d^*}{l_d^* + d_s}\right)^3\right] \qquad \text{Eq.8}$$

gives a slightly better law than Eq. 7 previously proposed: [6]

$$\Delta\lambda = S\,(n_s - n_{med})\left[1 - exp\left(-\frac{2d_s}{l_d}\right)\right] \qquad \text{Eq.7}$$

For this, we used the dipolar approximation for calculating the LSPR position of core-shell particles in water ($n_{med} = 1.333$) [7], (i) for a spherical gold core with radius 10 nm with shells of different thicknesses d_s and of refractive index $n_s = 1.55$, and (ii) for an ellipsoidal core corresponding to the average particle shape of sample (I), with the same shells. Figure S.9 shows the positions of the LSPR of the core-shell sphere and of the long wavelength LSPR of the core-shell ellipsoid, plotted with blue diamonds. The red and black curves are the best fit of these shifts, by using Eq.8 and Eq.7, respectively.

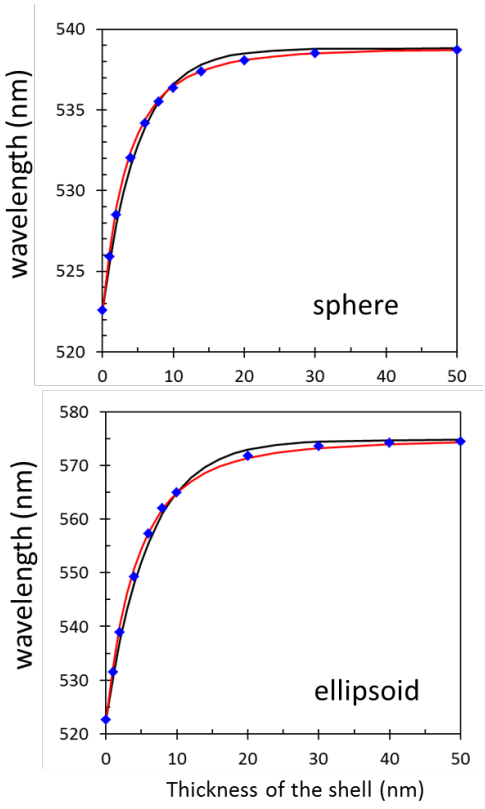

Fig.S.9. Blue diamonds: position of the LSPR calculated by use of the dipolar approximation. Black line: best fit using Eq.7. Red line: best fit using Eq.8. The parameters used in the calculations, given in *nm*, are the following. For the sphere: radius $R = 10$; $l_d = 10$, $l_d^* = 11$. For the ellipsoid: $a = 17.9$, $b = 13.6$, $c = 9.0$; $l_d = 12$, $l_d^* = 13.5$.

Part SI.8. Effect of the density of the molecule layer.

The refractive index of a biomolecule layer in a solvent is intermediate between that of the solvent and that of the dry layer, and varies linearly with its concentration[8,9]. In consequence, the optical response of an ellipsoid covered by a dense or a dilute biomolecule layer is unchanged for the same total number of molecules. Indeed, it can be calculated that the polarizability of a gold ellipsoid, with same dimensions as the average NP of sample (I) in water (here, the water RI was taken as $n = 1.33$) covered by a layer of 0.6 nm of dense biomolecule layer, with $n = 1.55$, is almost identical to the polarizability of the same gold ellipsoid covered, e.g. by a 2.4 ***nm*** layer 4 times less dense, with a refractive index (RI) equal to $n = 1.33 + (1.55 - 1.33)/4) = 1.385$, when compared to the NP without shell, as seen in Fig.S.10. This is similar to the case of ellipsometry, for which measured signals for a layer of thickness t and RI n on a surface depends only on the product $n \times t$.

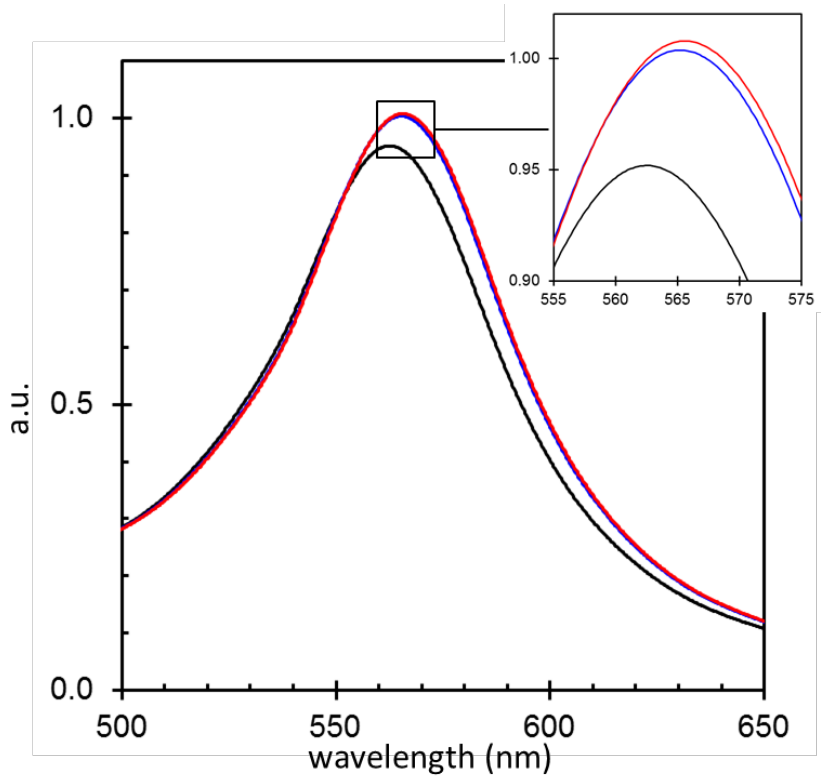

Fig.S.10. Polarizability of a core-shell ellipsoidal NP with dimensions $a = 17.9\,nm$, $b = 13.6\,nm$, $c = 9.0\,nm$. Black line: without shell; red line: with shell given by thickness $d_s = 0.6\,nm$ and $n = 1.55$; blue line: shell given by $d_s = 2.4\,nm$ and $n = 1.385$

Part SI.9. Comparison between the sample IV without biotin and with a layer of 0.6 nm biotin covering all the NPs.

Fig.S.11 gives the calculated TA spectrum for the sample (IV), either in water without shell (as drawn in main article in Fig.6.a), and the RA spectrum for all gold NPs covered by a biotin layer 0.6 nm thick with RI n=1.55.

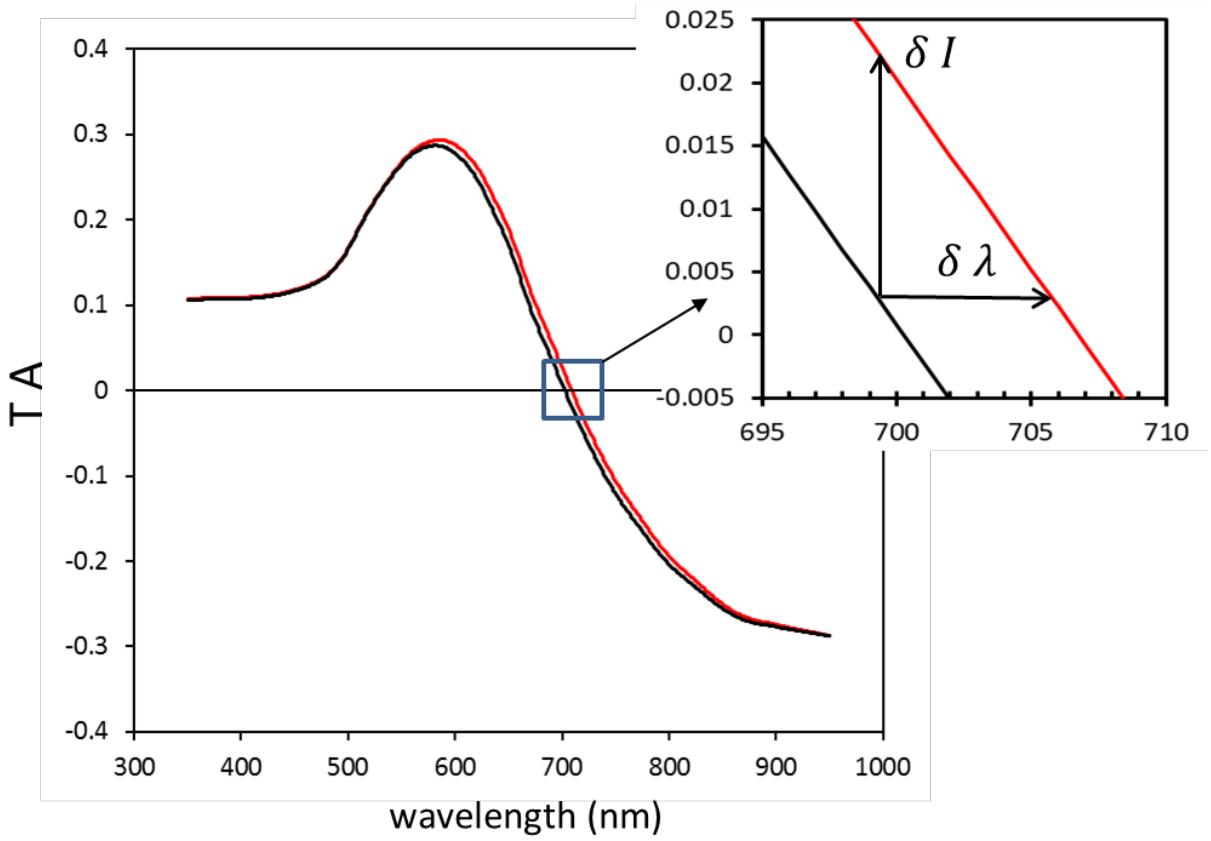

Fig S.11. Black curve: calculated transmission anisotropy spectrum (TAS) of sample (IV) in water. Red curve: calculated TAS for the same sample with each NP covered by a 0.6 nm of biotin.

Part SI.10. Optical response of a hetero-dimer Au NP / biomolecule, versus a core-shell (Au@biomolecule) NP

We compare three polarizabilities: one is a bare gold ellipsoid in water, the second is the same ellipsoid AuNP covered with a film of biomolecule of thickness d, and the third is a heterodimer (Au ellipsoid + biomolecule ellipsoid) with three different configurations (Fig. S.12). The volume of the biomolecule was taken equal to $V = 100\ \text{nm}^3$, i.e. that of the avidin molecule, and the half short axis c_b of the biomolecule ellipsoid was taken equal to 2 nm, the half short size of the avidin molecule. The parameters of the Au ellipsoid were taken equal to: $a = 25$ nm, $b = 20$ nm and $c = 13$ nm. The thickness d is chosen in order to have a shell with the same volume V, given by $t = V/A$, where $A = 4651\ \text{nm}^2$ is the area of the gold ellipsoid, calculated using the approximated expression proposed by Knud:[10]

$$A = 4\pi \left(\frac{a^p b^p + b^p c^p + c^p a^p}{3} \right)^{1/p}$$

with $p = 1.6075$. This gives a thickness $t = 0.0215$ nm.

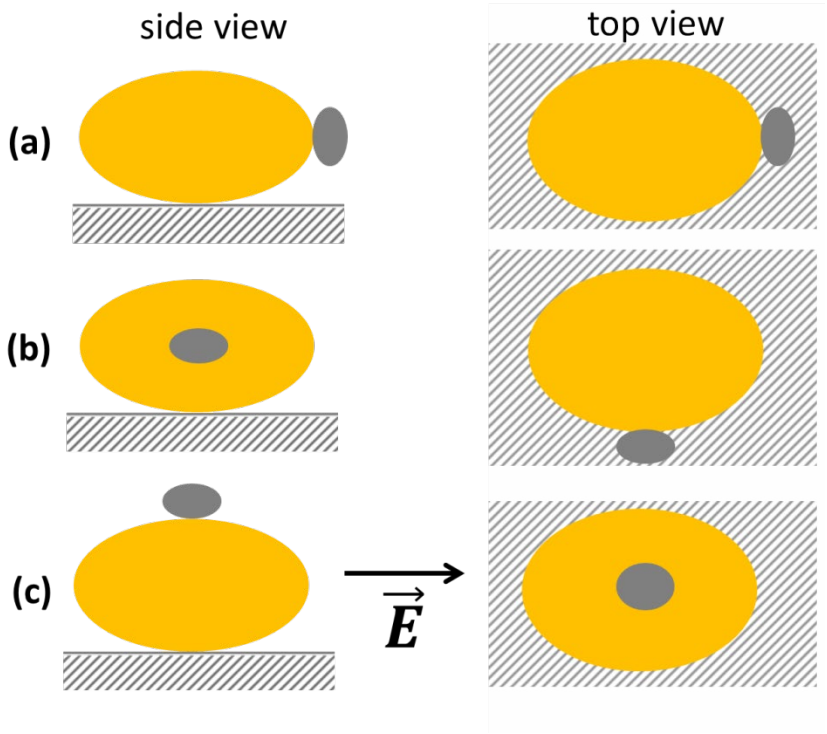

Fig.S.12. Diagram of the hereto-dimer Au NP / molecule, for three different configurations.

A straightforward algebraic development gives the following expression for the polarizability of the dimer:

$$\alpha_{\perp,\parallel}^{dimer}(\omega) = \frac{\alpha_1(\omega) + \alpha_2(\omega) - 2\, D_{\perp,\parallel}\, \alpha_1(\omega)\, \alpha_2(\omega)}{1 - {D_{\perp,\parallel}}^2\, \alpha_1(\omega)\, \alpha_2(\omega)}$$

where $\alpha_1(\omega)$ and $\alpha_2(\omega)$ are the polarizabilities in the direction of the incident electric field of the Au ellipsoid and of the avidin molecule considered as an ellipsoid, and $D_\perp$ and $D_\parallel$ are given by : $D_\parallel = -2/(4\pi\, d^3)$ and $D_\perp = 1/(4\pi\, d^3)$, d is the distance between the centers of the ellipsoids. Here$\parallel$ corresponds to the configuration (a) where the direction defined by the centers of the two ellipsoids is parallel to the applied electric field, whereas $\perp$ corresponds to configurations (b) and (c) where it is perpendicular.

The imaginary parts of the polarizability of the dimers are drawn in Fig. S.13. In the perpendicular (b) configuration, the change with respect to the bare Au NP is small, whereas it is intermediate for the parallel (a) configuration and large in the perpendicular (c) configuration. This is related to the distance d between the centers of both ellipsoids, and depends on the configuration. It should also be noted that the dipole approximation is not valid for too small values of d, e.g. for a flatter shape of the Au NP (configuration c), leading in this case to too large of a shift. Taking the average between the three configurations, the change drawn in red dashed line is not far from what is calculated for the core-shell NP in red continuous line, which shows that using this latter approach is reasonable to determine the effect of one single or of a few molecules adsorbed on the gold NP.

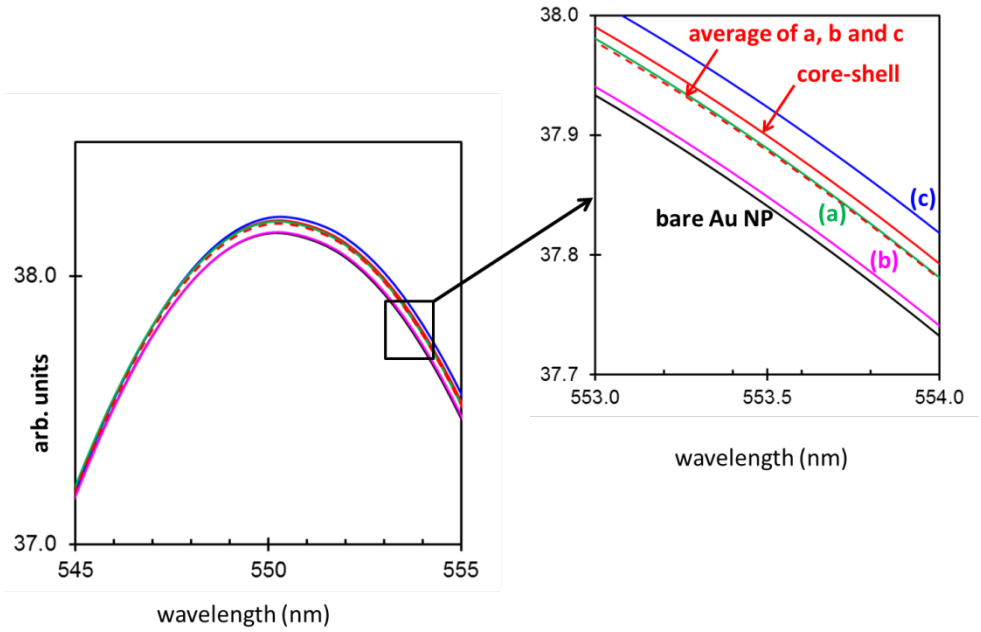

Fig.S.13. Polarizability of the hetero-dimers shown in Fig.S.12 for different configurations (indicated in the figure), compared with the core-shell ellipsoid and the bare Au ellipsoid.

However, the dipole approximation used in this calculation cannot account for the possible effect of the "hot spots" located between Au NPs neighbors, corresponding to the (a) and (b) configurations, where enhanced electric fields are expected, yielding a larger sensitivity to the adsorbed molecules.

[1] A.B. Tesler, L. Chuntonov, T. Karakouz, T.A. Bendikov, A. Vaskevich, I. Rubinstein, Tunable Localized Plasmon Transducers Prepared by Thermal Dewetting of Percolated Evaporated Gold Films, J. Phys. Chem. C. 115 (2011) 24642–24652. https://doi.org/10.1021/jp209114j.
[2] D.E. Aspnes, J.P. Harbison, A.A. Studna, L.T. Florez, Reflectance-difference spectroscopy system for real-time measurements of crystal growth, Applied Physics Letters. 52 (1988) 957. https://doi.org/10.1063/1.99240.
[3] P.B. Johnson, R.-W. Christy, Optical constants of the noble metals, Physical Review B. 6 (1972) 4370. https://doi.org/10.1103/PhysRevB.6.4370.
[4] Y. Borensztein, L. Delannoy, A. Djedidi, R.G. Barrera, C. Louis, Monitoring of the Plasmon Resonance of Gold Nanoparticles in Au/TiO ₂ Catalyst under Oxidative and Reducing Atmospheres, The Journal of Physical Chemistry C. 114 (2010) 9008–9021. https://doi.org/10.1021/jp101248h.
[5] U. Kreibig, M. Vollmer, Optical Properties of Metal Clusters, Springer, 1995.
[6] J.N. Anker, W.P. Hall, O. Lyandres, N.C. Shah, J. Zhao, R.P. Van Duyne, Biosensing with plasmonic nanosensors, Nature Materials. 7 (2008) 442–453. https://doi.org/10.1038/nmat2162.
[7] C.F. Bohren, D.R. Huffman, Absorption and scattering of light by small particles, Wiley-VCH, 2004.

[8] J. Vörös, The Density and Refractive Index of Adsorbing Protein Layers, Biophysical Journal. 87 (2004) 553–561. https://doi.org/10.1529/biophysj.103.030072.
[9] H. Zhao, P.H. Brown, P. Schuck, On the Distribution of Protein Refractive Index Increments, Biophys J. 100 (2011) 2309–2317. https://doi.org/10.1016/j.bpj.2011.03.004.
[10] http://www.numericana.com/answer/ellipsoid.htm#ellipsoid.